Experimental Design in Global Compartmental Analysis of Reversible Intramolecular Two-State Excited-State Processes with Added Quencher

ARTICLE *in* THE JOURNAL OF PHYSICAL CHEMISTRY A · MARCH 1997

Impact Factor: 2.69 · DOI: 10.1021/jp962147b

5 AUTHORS, INCLUDING:

GB Dutt
Bhabha Atomic Research Centre
75 PUBLICATIONS **1,633** CITATIONS
SEE PROFILE

Andrzej Kowalczyk
Nicolaus Copernicus University
141 PUBLICATIONS **4,549** CITATIONS
SEE PROFILE

Frans C De Schryver
University of Leuven
670 PUBLICATIONS **21,243** CITATIONS
SEE PROFILE

Marcel Ameloot
Hasselt University
220 PUBLICATIONS **3,489** CITATIONS
SEE PROFILE

ARTICLES

Experimental Design in Global Compartmental Analysis of Reversible Intramolecular Two-State Excited-State Processes with Added Quencher

G. Bhaskar Dutt,[†,||] Noël Boens,*[,†,⊥] Andrzej Kowalczyk,[†,‡,▽] Frans C. De Schryver,[†] and Marcel Ameloot[§]

Department of Chemistry, Katholieke Universiteit Leuven, B-3001 Heverlee, Belgium, and Limburgs Universitair Centrum, B-3590 Diepenbeek, Belgium

Received: July 17, 1996; In Final Form: November 29, 1996[⊗]

Although reversible intramolecular two-state excited-state processes without *a priori* information are unidentifiable, bounds on the excited-state rate constants k_{ij} can be specified when a quencher is used [Van Dommelen et al. *J. Phys. Chem.* **1993**, *97*, 11738]. These limits can be obtained by a scanning procedure consisting of a series of global compartmental analyses of a fluorescence decay surface in which one of the rate constants k_{ij} is held fixed at different preset values. The theory requires that the rate constants of quenching (k_{Q1}, k_{Q2}) for the two excited species have different values. In the present paper, computer-generated fluorescence decay surfaces are used to investigate the criteria under which reliable estimates of the bounds on the rate constants k_{ij} can be obtained. If the values of k_{Q1} and k_{Q2} are substantially different, reliable estimates are obtained. If k_{Q1} and k_{Q2} are nearly equal in value, the quality of the estimates of the bounds depends on the combinations of the values of the rate constants k_{ij}. It may happen that no reliable limits for the rate constants can be obtained so that another quencher is required. A test procedure based on a limited number of decay traces is described which allows one to assess the appropriateness of the quencher for the given excited-state process.

1. Introduction

In recent times, the global compartmental analysis method[1−24] has been successfully applied to determine excited-state kinetics from fluorescence decay surfaces. Studies on the structural identifiability and corresponding experimental investigations have been carried out on intermolecular[1−18] as well as intramolecular[19−24] excited-state processes. It has been demonstrated that simultaneous (global) analysis[25−30] of multiple fluorescence decay curves, measured along different experimental axes, such as emission/excitation wavelength, concentration, temperature, pH, etc. enhances the parameter recovery and model discrimination power compared to single-curve analysis. In simultaneous analysis, common model parameters are partly or totally linked over the fluorescence decay surface. Using the global compartmental analysis method, one can determine the rate constants of the excited-state processes and spectral absorption and emission parameters. In earlier contributions concerning intramolecular two-state excited-state processes with[20] and without[21] added quencher, the structural identifiability problem has been discussed. It has been found that intramolecular two-state excited-state processes are unidentifiable without *a priori* information. By using the so-called scanning procedure,[22,23] upper and lower limits on the rate constants can be determined for intramolecular two-state excited-state processes in the presence of added quencher provided that the rate constants of quenching of the two excited states have different values. It is also possible to construct species-associated emission and excitation spectra.[22,23]

In this report, we use computer-generated fluorescence decay surfaces to investigate how the proximity of the two values of the quenching rate constants affects the reliability of the estimates of the bounds on the excited-state rate constants. This study allows us to propose a rational strategy for designing time-resolved fluorescence experiments of reversible intramolecular two-state excited-state processes.

2. Theory

2.1. Fluorescence Decay Kinetics. Consider an intramolecular system consisting of two distinct types of excited-state species with added quencher as depicted in Scheme 1. The rate constant for deactivation of i^* ($i = 1$ and 2) in the absence of quencher is denoted by k_{0i}. This composite rate constant k_{0i} is the sum of the rate constants for fluorescence and nonradiative decay for excited state i^*. When a quencher Q is added to the system, the deactivation processes is accelerated by $k_{Qi}[Q][i^*]$ for excited state i^*. It is assumed that the added quencher does not alter the ground-state equilibrium and that the quenching rate constants k_{Qi} represent an adequate description of the kinetics.

The decay of fluorescence emitted by such a system after δ-pulse excitation can be written as a sum of two exponentials:

* To whom all correspondence should be addressed.
† Katholieke Universiteit Leuven.
‡ On leave from the Institute of Physics, Nicholas Copernicus University, 87-100 Torun, Poland.
§ Limburgs Universitair Centrum.
|| G.B.D. has a junior Fellowship of the University Research Fund of the Katholieke Universiteit Leuven.
⊥ N.B. is an Onderzoeksdirecteur of the Nationaal Fonds voor Wetenschappelijk Onderzoek (NFWO, Belgium).
▽ A.K. has a Senior Fellowship of the University Research Fund of the Katholieke Universiteit Leuven.
⊗ Abstract published in *Advance ACS Abstracts,* February 15, 1997.

S1089-5639(96)02147-0 CCC: $14.00

SCHEME 1

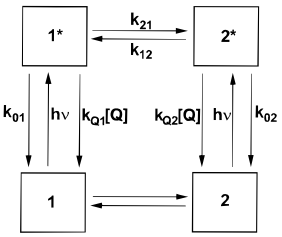

$$f(\lambda^{em},\lambda^{ex},t) = \alpha_1 \exp(\gamma_1 t) + \alpha_2 \exp(\gamma_2 t), \quad t \geq 0 \qquad (1)$$

The exponential factors $\gamma_{1,2}$ are given by[20]

$$\gamma_{1,2} = -1/2\{S_1 + S_2 + (k_{Q1} + k_{Q2})[Q] \mp [[S_1 - S_2 + (k_{Q1} - k_{Q2})[Q]]^2 + 4P]^{1/2}\} \qquad (2)$$

and are related to the decay times $\tau_{1,2}$ according to

$$\gamma_{1,2} = -1/\tau_{1,2} \qquad (3)$$

with

$$S_1 = k_{01} + k_{21} \qquad (4a)$$

$$S_2 = k_{02} + k_{12} \qquad (4b)$$

$$P = k_{12}k_{21} \qquad (4c)$$

Since all rate constants k_{ij} are nonnegative, S_1, S_2, and P also are nonnegative. The exponential factors $\gamma_{1,2}$ depend on all rate constants and [Q] while the preexponential factors $\alpha_{1,2}$ are dependent on all rate constants, [Q], the spectral parameters $\tilde{\boldsymbol{b}}(\lambda^{ex})$, and $\tilde{\boldsymbol{c}}(\lambda^{em})$.[20]

$\tilde{\boldsymbol{b}}(\lambda^{ex})$ is the 2 × 1 vector with elements $\tilde{b}_i(\lambda^{ex})$ defined by

$$\tilde{b}_i = b_i/(b_1 + b_2), \quad \text{for } i = 1, 2 \qquad (5)$$

where b_i denotes the concentration of i^* at time zero.

$$b_i = [i^*]_{t=0} \qquad (6)$$

which, in the low excitation limit and when Beer's law is valid, is proportional to the ground-state absorbance.

$\tilde{\mathbf{c}}(\lambda^{em})$ is the 1 × 2 vector of the normalized emission weighting factors $\tilde{c}_i(\lambda^{em})$:

$$\tilde{c}_i = c_i/(c_1 + c_2), \quad \text{for } i = 1, 2 \qquad (7)$$

$c_i(\lambda^{em})$ of species i^* at λ^{em} is defined as[3]

$$c_i(\lambda^{em}) = k_{Fi}\int_{\Delta\lambda^{em}} \rho_i(\lambda^{em})\, d\lambda^{em} \qquad (8)$$

k_{Fi} is the fluorescence rate constant of species i^*, $\Delta\lambda^{em}$ is the emission wavelength interval where the fluorescence is monitored, and $\rho_i(\lambda^{em})$ is the spectral emission density of species i^* at λ^{em} defined by

$$\rho_i(\lambda^{em}) = \frac{F_i(\lambda^{em})}{\int F_i(\lambda^{em})\, d\lambda^{em}} \qquad (9)$$

where the integration extends over the whole steady-state fluorescence spectrum F_i of species i^*. $\tilde{\boldsymbol{b}}(\lambda^{ex})$ can be linked over decay curves collected at the same excitation wavelength, whereas $\tilde{\boldsymbol{c}}(\lambda^{ex})$ can be linked over decay curves obtained at the same emission wavelength.

2.2. Identifiability Conditions. The following conditions[20] have to be satisfied to make a reversible intramolecular two-state excited-state system identifiable. First, the fluorescence decay surface must include at least one set of decay traces measured for a minimum of three different quencher concentrations at the same excitation/emission wavelength. One of the quencher concentrations may be equal to zero. Second, the values of the rate constants of quenching of the two excited species must be different. Third, at least one of the rate constants k_{ij}, which is not a rate constant of quenching, must be known *a priori*. If this last information is not available, it is possible to determine the combinations of the rate constants k_{ij} given by eq 4 which subsequently allows upper and lower limits on the rate constants to be specified.[22]

$$0 < k_{01} < S_1 - P/S_2 \qquad (10a)$$

$$P/S_2 < k_{21} < S_1 \qquad (10b)$$

$$0 < k_{02} < S_2 - \mathrm{P}/S_1 \qquad (10c)$$

$$\mathrm{P}/S_1 < k_{12} < S_2 \qquad (10d)$$

Now we will discuss how these combinations of rate constants can be obtained from the decay times of fluorescence decay traces collected at different quencher concentrations. The following combinations: of decay times are assumed to be known from the experiment: $\sigma_1 \equiv \gamma_1 + \gamma_2$ and $\sigma_2 \equiv \gamma_1\gamma_2$ Both σ_1 and σ_2 are functions of S_i, P, and k_{Qi} (i = 1 and 2).

$$\sigma_1 = -(S_1 + S_2) - (k_{Q1} + k_{Q2})[Q] \qquad (11)$$

$$\sigma_2 = k_{Q1}k_{Q2}[Q]^2 + (k_{Q2}S_1 + k_{Q1}S_2)[Q] + S_1S_2 - \mathrm{P} \qquad (12)$$

As eq 11 is linear in [Q], it is possible get a slope A and intercept B using only two different concentrations of Q:

$$A = -(k_{Q1} + k_{Q2}) \qquad (13)$$

$$B = -(S_1 + S_2) \qquad (14)$$

Equation 12 is quadratic in [Q]. Therefore, three different Q concentrations are sufficient to determine the coefficients C, D, and E of this parabola:

$$C = k_{Q1}k_{Q2} \qquad (15)$$

$$D = k_{Q2}S_1 + k_{Q1}S_2 \qquad (16)$$

$$E = S_1S_1 - \mathrm{P} \qquad (17)$$

Equations 13 and 15 provide two values which can not be uniquely associated with k_{Q1} or k_{Q2}.

If, however, one arbitrarily marks one value as k_{Q1} and the other as k_{Q2}, eqs 14 and 16 provide values for S_1 and S_2 which are always correctly associated with, respectively, k_{Q1} and k_{Q2}. The theory predicts that $S_1 + S_2$ will always be well defined, but the numerical recovery of the individual S_1 and S_2 will depend on the relative values of k_{Qi}. Indeed, eqs 14 and 16 define two lines in the $\{S_1S_2\}$ plane:

$$S_1 = -B - S_2 \qquad (18)$$

$$S_1 = D/k_{Q2} - (k_{Q1}/k_{Q2})S_2 \qquad (19)$$

In the present contribution, two sets of quenching rate constants are considered: one with $k_{Q1} = 7\ \mathrm{M}^{-1}\ \mathrm{ns}^{-1}$and k_{Q2}

$= 6\ M^{-1}\ ns^{-1}$ and another with $k_{Q1} = 7\ M^{-1}\ ns^{-1}$ and $k_{Q2} = 1\ M^{-1}\ ns^{-1}$. The system of eqs 18 and 19 is ill conditioned in the first case because the angle between these two lines is about 4.4°, while in the second case the crossing point is well determined as both lines cross at an angle 36.9°. P can then be determined from eq 17. Note that $0 \le P \le S_1\ S_2$.

For irreversible intramolecular excited-state processes where $P = 0$, the values of S_1 and S_2 can be determined from eqs 14 and 17 without the need to use any quencher.

In global compartmental analysis one can fit directly for S_1, S_2, P, k_{Q1}, and k_{Q2} and subsequently the limits for each rate constant k_{ij} can be evaluated using eq 10. In the present paper, however, we use the scanning procedure[22,23] described below to obtain the estimates of S_1, S_2, P, k_{Q1}, and k_{Q2}. Although more time consuming, the scanning procedure was chosen to analyze the data because it allows one to assess the reliability of S_1, S_2, P, k_{Q1}, and k_{Q2} (see section 2.3). Such information is essential if there is a risk that the equations describing a system are ill conditioned (*i.e.*, when the values of the quenching rate constants are very similar).

2.3. Use of the Scanning Procedure to Obtain Rate Constant Limits. By using the scanning procedure,[22,23] that is, by keeping one of the rate constants k_{ij} fixed at different preset values while the other parameters are freely adjustable in the analysis, it is possible to estimate values of the remaining k_{ij}, k_{Q1}, k_{Q2}, $\tilde{b}_1$, and $\tilde{c}_1$. From the values of the scanned rate constant and the corresponding estimated values of the other rate constants, it is possible to calculate S_1, S_2, and P (eq 4). The graphs of S_1, S_2, and P *vs* the scanned rate constant should exhibit a limited plateau region because of the nonnegativity of the rate constant values k_{ij}. The limits on k_{ij} are calculated according to eq 20,

$$0 < k_{01} < \langle S_1 - P/S_2 \rangle \tag{20a}$$

$$\langle P/S_2 \rangle < k_{21} < \langle S_1 \rangle \tag{20b}$$

$$0 < k_{02} < \langle S_2 - P/S_1 \rangle \tag{20c}$$

$$\langle P/S_1 \rangle < k_{12} < \langle S_2 \rangle \tag{20d}$$

where $\langle\ \rangle$ denotes the average over the plateau region. Since this type of averaging takes into account the correlations between S_1, S_2, and P, this procedure is followed in this paper. Propagated errors on S_1, S_2, and P were calculated using the standard deviations of the individual k_{ij} available from the global compartmental analysis. They were then compared with the sample standard deviations describing the spread of S_1, S_2, and P around their mean values within the plateaus. The larger of each pair was taken as the error on $\langle S_1 \rangle$, $\langle S_2 \rangle$, and $\langle P \rangle$. These error values were eventually used to calculate the propagated errors on the limits of k_{ij}.

Note that the lower and upper bounds calculated for the scanned rate constant according to eq 20 should match the visually determined lower and upper bounds of the plateau regions of the graphs of S_1, S_2, and P plotted as a function of the scanned rate constant.[22,23] Lack of such consistency provides a very important test indicating that the values of S_1, S_2, and P might not be properly recovered and that therefore the calculated limits on k_{ij} are unreliable. We shall use this test as a criterion to judge the feasibility of obtaining reliable bounds on k_{ij}.

3. Methods

3.1. Program Implementation. The global compartmental analysis of the fluorescence decay surface of species undergoing intramolecular excited-state processes was implemented in the existing general global analysis program[30] based on Marquardt's[31] algorithm. For reversible intramolecular two-state excited-state processes with added quencher, the global fitting parameters are k_{01}, k_{21}, k_{02}, k_{12}, k_{Q1}, k_{Q2}, $\tilde{b}_1(\lambda^{ex})$, and $\tilde{c}_1(\lambda^{em})$. Each decay trace has an additional local scaling factor. A detailed description of the program implementation of global compartmental analysis has been given elsewhere.[20] The fitting parameters were estimated by minimizing the global reduced χ_g^2:

$$\chi_g^2 = \sum_l^q \sum_i w_{li}(y_{li}^o - y_{li}^c)^2/\nu \tag{21}$$

where the index l sums over q experiments, and the index i sums over the appropriate channel limits for each individual experiment. y_{li}^o and y_{li}^c denote respectively the observed (synthetic) and calculated (fitted) values corresponding to the ith channel of the lth experiment. w_{li} is the corresponding statistical weight. ν represents the number of degrees of freedom for the entire multidimensional fluorescence decay surface. It is crucial that all fitting parameters are subject to simple range constraints on their values. The problem of minimizing χ_g^2 can be stated mathematically as follows:

$$\text{minimize } \chi_g^2(x) \text{ for all } x, \quad x \in R^n \tag{22}$$

$$\text{subject to } s_j \le x_j \le t_j \quad j = 1, 2, \ldots n$$

with n the number of adjustable parameters. This format assumes that upper and lower constraints exist on all fitting parameters. Restrictions on the values of a particular fitting parameter j can be removed by allowing very large negative and positive values, respectively, for s_j and t_j. For all rate constants, s_j was set at $-0.01\ ns^{-1}$, and for the local scaling factors, s_j was set at 0. The default constraints on $\tilde{b}_1$ and $\tilde{c}_1$are $-0.5 \le (\tilde{b}_1, \tilde{c}_1) \le 1.5$. Small negative s_j prevent oscillations in the nonlinear least-squares search, which would occur if the values of the fitting parameters were forced to be nonnegative. The global reduced χ_g^2 statistic and its corresponding normal deviate $Z_{\chi_g^2}$ provided numerical goodness-of-fit criteria for the entire fluorescence decay surface:

$$Z_{\chi_g^2} = ({}^1/_2\nu)^{1/2}(\chi_g^2 - 1) \tag{23}$$

By using $Z_{\chi_g^2}$, the goodness-of-fit of analyses with different ν can be readily compared. Additional goodness-of-fit criteria are described elsewhere.[32]

3.2. Synthetic Data Generation. Synthetic sample decays were generated by convolution of $f(t)$ with an instrument response function. The preexponential factors $\alpha_{1,2}$ and the corresponding decay times $\tau_{1,2}$ of the biexponential decays were computed from the rate constants k_{ij}, k_{Q1}, k_{Q2}, $\tilde{b}_1$, $\tilde{c}_1$ and [Q] by a dedicated computer program. The quencher concentrations used were 0, 4, 10, and 20 mM unless specified otherwise. A value of 0.8 was chosen for $\tilde{b}_1$, whereas $\tilde{c}_1$ was varied from 0.0 to 1.0 in steps of 0.1. The computer-generated fluorescence decay surface mimics that when fluorescence decays at various quencher concentrations are collected at different emission wavelengths due to excitation at a single wavelength. All computer-generated decays had 500 data points and 10 000 counts in the peak channel. The time increment per channel was chosen to ensure that the final decay intensity was about 5% or less of the peak intensity. Full details of the decay data simulations are given elsewhere.[33] The synthetic data genera-

TABLE 1: Simulation Values for the Rate Constants k_{ij} (in ns^{-1}), k_{Q1}, k_{Q2} and S_1, S_2, and P for the Intramolecular Two-State Excited-State Processes Depicted in Scheme 1. Limits on the Rate Constants k_{ij} (in ns^{-1}) Calculated According to Eq 10 Using the Simulation Values of S_1, S_2, and P

	Section 1	
$k_{01} = 0.02$	$S_1 = 0.17$ ns^{-1}	$0 < k_{01} < 0.0597$
$k_{21} = 0.15$	$S_2 = 0.34$ ns^{-1}	$0.1103 < k_{21} < 0.17$
$k_{02} = 0.09$	P = 0.0375 ns^{-2}	$0 < k_{02} < 0.1194$
$k_{12} = 0.25$		$0.2206 < k_{12} < 0.34$
	Section 2	
$k_{01} = 0.16$	$S_1 = 0.17$ ns^{-1}	$0 < k_{01} < 0.1671$
$k_{21} = 0.01$	$S_2 = 0.34$ ns^{-1}	$0.0029 < k_{21} < 0.17$
$k_{02} = 0.24$	P = 0.001 ns^{-2}	$0 < k_{02} < 0.3341$
$k_{12} = 0.10$		$0.0059 < k_{12} < 0.34$
	Section 3	
$k_{01} = 0.07$	$S_1 = 0.17$ ns^{-1}	$0 < k_{01} < 0.1637$
$k_{21} = 0.1$	$S_2 = 0.16$ ns^{-1}	$0.0063 < k_{21} < 0.17$
$k_{02} = 0.15$	P = 0.001 ns^{-2}	$0 < k_{02} < 0.1541$
$k_{12} = 0.01$		$0.0059 < k_{12} < 0.16$
	Section 4	
$k_{01} = 0.16$	$S_1 = 0.17$ ns^{-1}	$0 < k_{01} < 0.1699$
$k_{21} = 0.01$	$S_2 = 0.80$ ns^{-1}	$0.0001 < k_{21} < 0.17$
$k_{02} = 0.79$	P = 0.0001 ns^{-2}	$0 < k_{02} < 0.7994$
$k_{12} = 0.01$		$0.0006 < k_{12} < 0.80$
	Section 5	
$k_{01} = 0.3$	$S_1 = 0.17$ ns^{-1}	$0 < k_{01} < 0.0440$
$k_{21} = 0.14$	$S_2 = 0.80$ ns^{-1}	$0.1260 < k_{21} < 0.17$
$k_{02} = 0.08$	P = 0.1008 ns^{-2}	$0 < k_{02} < 0.2071$
$k_{12} = 0.72$		$0.5929 < k_{12} < 0.80$
(a) $k_{Q1} = 7$ M^{-1} ns^{-1}	$k_{Q2} = 1$ M^{-1} ns^{-1}	
(b) $k_{Q1} = 7$ M^{-1} ns^{-1}	$k_{Q2} = 6$ M^{-1} ns^{-1}	

tions and all global compartmental analyses were carried out on an IBM RISC System/6000 computer.

3.3. Data Analysis. The fluorescence decay surface to be analyzed in each case comprised 44 decay curves (at 11 $\tilde{c}_1$ values and four quencher concentrations). The fluorescence decay surface was globally analyzed in terms of k_{ij}, k_{Q1}, k_{Q2}, $\tilde{b}_1$, and $\tilde{c}_1$. In all of the 44 decays, the parameters k_{ij}, k_{Q1}, k_{Q2}, and $\tilde{b}_1$ were linked over the entire fluorescence decay surface while the 11 $\tilde{c}_1$ parameters were linked over four different quencher concentrations. From a previous study,[22] it was found that it is sufficient to scan one rate constant to obtain plateau values of S_1, S_2, and P and to subsequently estimate bounds on the rate constants k_{ij}. It was also found that it is less tedious to scan k_{01} (or k_{02}) instead of k_{21} (or k_{12}) because k_{01} (or k_{02}) has only an upper limit whereas k_{21} (or k_{12}) has both upper and lower bounds. So in all cases global compartmental analyses were performed by keeping k_{01} fixed at different preset values.

4. Results

The purpose of the investigation is to determine how the proximity of the values of the two quenching rate constants k_{Q1} and k_{Q2} influences the recovery of the parameters S_1, S_2, P, k_{Q1}, and k_{Q2} and how well one can estimate the limits on the rate constants k_{ij}. Therefore, we consider five different combinations of S_1, S_2, and P. Note that by definition P is restricted between 0 and S_1S_2. For each case, two different subcases are investigated. In the first subcase the values of the two quenching rate constants are far apart ($k_{Q1} = 7$ M^{-1} ns^{-1} and $k_{Q2} = 1$ M^{-1} ns^{-1}) while in the second subcase they are close ($k_{Q1} = 7$ M^{-1} ns^{-1} and $k_{Q2} = 6$ M^{-1} ns^{-1}). The simulation values of the rate constants k_{ij}, k_{Q1}, k_{Q2} and the simulation values of S_1, S_2, and P (eq 4) are given in Table 1. The theoretical limits (eq 10) on the rate constants k_{ij} are also compiled in that table.

TABLE 2: Average Values of k_{Q1}, k_{Q2} (in M^{-1} ns^{-1}), S_1, S_2 (in ns^{-1}), and P (in ns^{-2}) and Their Errors Estimated by the Scanning Procedure of the Fluorescence Decay Surface Generated with the Simulation Values of Table 1 with $k_{Q1} = 7$ M^{-1} ns^{-1} and $k_{Q2} = 1$ M^{-1} ns^{-1}. Limits on the Rate Constants k_{ij} (in ns^{-1}) Are Calculated According to Eq 20

Section 1	
$S_1 = 0.171 \pm 0.007$	$0 < k_{01} < 0.06 \pm 0.01$
$S_2 = 0.335 \pm 0.007$	$0.111 \pm 0.006 < k_{21} < 0.171 \pm 0.007$
P $= 0.037 \pm 0.002$	$0 < k_{02} < 0.12 \pm 0.02$
$k_{Q1} = 7.0 \pm 0.1$	$0.22 \pm 0.01 < k_{12} < 0.335 \pm 0.007$
$k_{Q2} = 1.1 \pm 0.2$	
Section 2	
$S_1 = 0.1683 \pm 0.0005$	$0 < k_{01} < 0.1666 \pm 0.0006$
$S_2 = 0.342 \pm 0.002$	$0.0021 \pm 0.0002 < k_{21} < 0.1683 \pm 0.0005$
P $= 0.0007 \pm 0.0001$	$0 < k_{02} < 0.338 \pm 0.002$
$k_{Q1} = 6.87 \pm 0.04$	$0.0042 \pm 0.0005 < k_{12} < 0.342 \pm 0.002$
$k_{Q2} = 0.8 \pm 0.1$	
Section 3	
$S_1 = 0.1679 \pm 0.0002$	$0 < k_{01} < 0.1623 \pm 0.0002$
$S_2 = 0.1603 \pm 0.0003$	$0.0056 \pm 0.0001 < k_{21} < 0.1679 \pm 0.0002$
P $= 0.00089 \pm 0.00002$	$0 < k_{02} < 0.1549 \pm 0.0003$
$k_{Q1} = 6.92 \pm 0.03$	$0.0053 \pm 0.0001 < k_{12} < 0.1603 \pm 0.0003$
$k_{Q2} = 1.02 \pm 0.01$	
Section 4	
$S_1 = 0.1702 \pm 0.0002$	$0 < k_{01} < 0.1701 \pm 0.0002$
$S_2 = 0.800 \pm 0.002$	$0.0002 \pm 0.0001 < k_{21} < 0.1702 \pm 0.0002$
P $= 0.00014 \pm 0.00008$	$0 < k_{02} < 0.800 \pm 0.002$
$k_{Q1} = 7.01 \pm 0.01$	$0.0008 \pm 0.0005 < k_{12} < 0.800 \pm 0.002$
$k_{Q2} = 1.0 \pm 0.2$	
Section 5	
$S_1 = 0.18 \pm 0.03$	$0 < k_{01} < 0.04 \pm 0.02$
$S_2 = 0.82 \pm 0.03$	$0.14 \pm 0.02 < k_{21} < 0.18 \pm 0.03$
P $= 0.11 \pm 0.02$	$0 < k_{02} < 0.2 \pm 0.1$
$k_{Q1} = 7.0 \pm 0.1$	$0.6 \pm 0.1 < k_{12} < 0.82 \pm 0.03$
$k_{Q2} = 1.1 \pm 0.2$	

TABLE 3: Average Values of k_{Q1}, k_{Q2} (in M^{-1} ns^{-1}), S_1, S_2 (in ns^{-1}), and P (in ns^{-2}) and Their Errors Estimated by the Scanning Procedure of the Fluorescence Decay Surface Generated with the Simulation Values of Table 1.2 with $k_{Q1} = 7$ M^{-1} ns^{-1} and $k_{Q2} = 6$ M^{-1} ns^{-1}. Limits on the Rate Constants k_{ij} (in ns^{-1}) Are Calculated According to Eq 20

$S_1 = 0.177 \pm 0.003$	$0 < k_{01} < 0.171 \pm 0.002$
$S_2 = 0.332 \pm 0.003$	$0.007 \pm 0.001 < k_{21} < 0.177 \pm 0.003$
P $= 0.0022 \pm 0.0005$	$0 < k_{02} < 0.320 \pm 0.006$
$k_{Q1} = 7.14 \pm 0.02$	$0.012 \pm 0.002 < k_{12} < 0.332 \pm 0.003$
$k_{Q2} = 6.02 \pm 0.06$	

4.1. Systems with $S_1 = 0.17$ ns^{-1}, $S_2 = 0.34$ ns^{-1}, and $P = 0.0375$ ns^{-2}. In this section we are studying a system in which S_1 and S_2 are well separated with $P/S_1S_2 = 0.65$. The decay time values as a function of [Q] for the two sets of quenching rate constants are shown in Figure 1. At low $\tilde{c}_1$ values, the preexponential factors corresponding to the short decay times are negative, whereas at higher $\tilde{c}_1$ values all preexponential factors are positive. During the scanning procedure the value of k_{01} was kept fixed at different preset values from 0.001 to 0.20 ns^{-1}.

4.1.a. $k_{Q1} = 7$ M^{-1} ns^{-1} and $k_{Q2} = 1$ M^{-1} ns^{-1}. The values of S_1, S_2, P, k_{Q1}, and k_{Q2} obtained as a function of the scanned rate constant k_{01} are shown in Figure 2. Visually well-defined plateaus are obtained for S_1, S_2, P, k_{Q1}, and k_{Q2} up to $k_{01} = 0.06$ ns^{-1} after which they start to deviate. The upper limit on k_{01} calculated by eq 20a (0.06 ns^{-1}) corresponds with all the visually determined limits. For the k_{01} region where plateaus are found, the fits as judged by $Z_{\chi^2_R}$ are acceptable. The values of S_1, S_2, P, k_{Q1}, and k_{Q2} averaged over the plateaus (Table 2.1) agree well with the simulation values of Table 1. The limits on k_{ij} calculated according to eq 20 (Table 2.1) are also in good agreement with the simulation values.

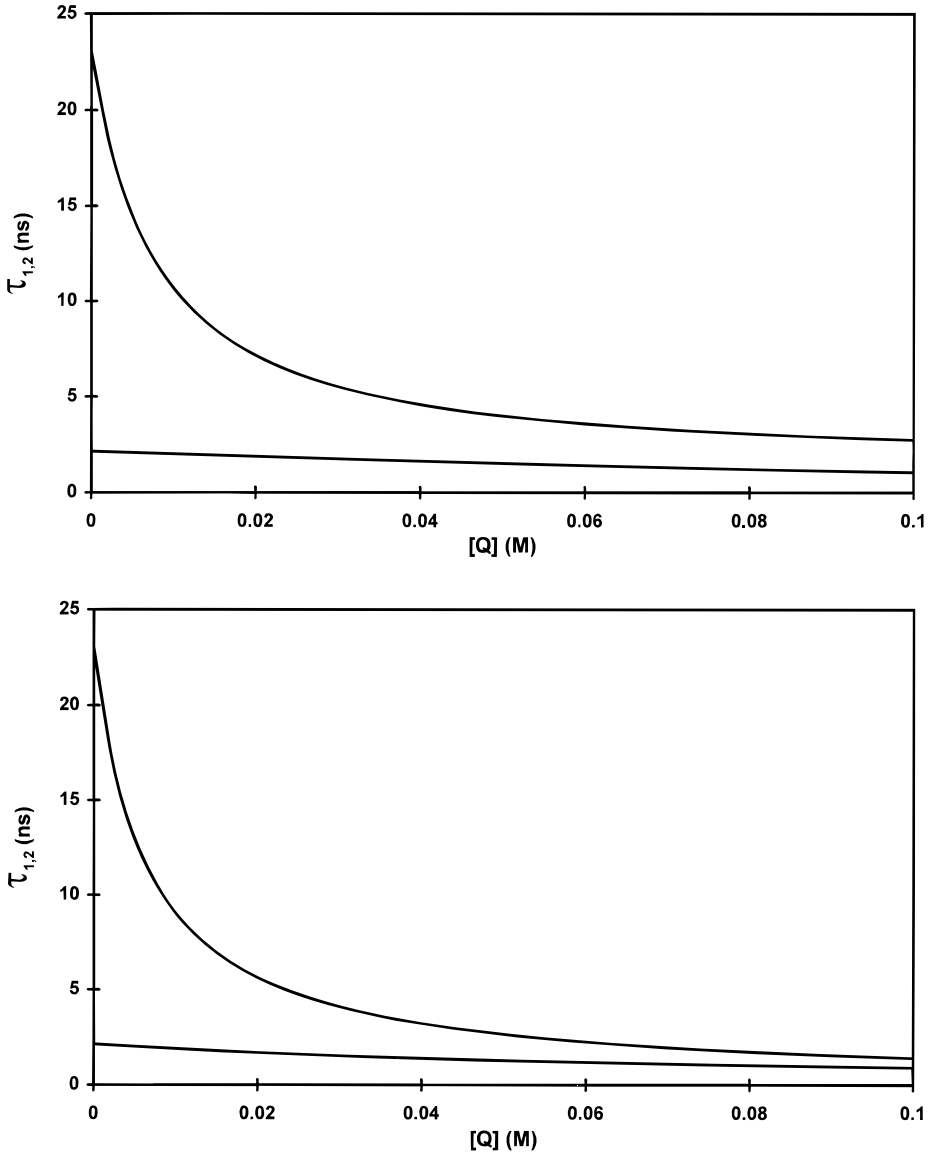

Figure 1. Decay times (τ_1 and τ_2) as a function of quencher concentration corresponding to case 4.1 ($S_1 = 0.17$ ns^{-1}, $S_2 = 0.34$ ns^{-1}, and $P = 0.0375$ ns^{-2}): (a) $k_{Q1} = 7$ M^{-1} ns^{-1} and $k_{Q2} = 1$ M^{-1} ns^{-1} (case 4.1.a). (b) $k_{Q1} = 7$ M^{-1} ns^{-1} and $k_{Q2} = 6$ M^{-1} ns^{-1} (case 4.1.b).

When the [Q] range is limited between 0 and 4 mM (0, 1, 2, and 4 mM, see Figure 1a for the decay time values), the values of S_1, S_2, k_{Q1}, and k_{Q2} obtained as a function of the scanned rate constant k_{01} (Figure 3) do not exhibit any plateaus. Therefore, it is impossible to calculate limits on k_{ij}. Note that the constancy of $(S_1 + S_2)$ explains the symmetry of the plots of S_1 and S_2.

4.1.b. $k_{Q1} = 7\ M^{-1}\ ns^{-1}$ *and* $k_{Q2} = 6\ M^{-1}\ ns^{-1}$. Unlike in the previous case, the two quenching rate constants are not well separated. As is evident from Figure 4, no plateaus are observed in the plots of S_1, S_2, P, k_{Q1}, and k_{Q2} as a function of the scanned rate constant k_{01}. Hence, no reliable limits on k_{ij} can be calculated. Extending the [Q] range up to 0.1 M (0, 0.02, 0.04, 0.1 M, see Figure 1b for $\tau_{1,2}$ values) does not result in plateaus for S_1, S_2, P, k_{Q1}, and k_{Q2} as a function of k_{01} (figure not shown). The symmetry of S_1 and S_2 in Figure 4a is explained by the constancy of $(S_1 + S_2)$.

4.2. Systems with $S_1 = 0.17$ ns^{-1}, $S_2 = 0.34$ ns^{-1}, and $P = 0.001$ ns^{-2}. The values of S_1 and S_2 are the same as in the previous section, but the value of P is much smaller ($P/S_1S_2 = 0.017$). The aim is to investigate how a small value of P affects the recovery of the parameters S_1, S_2, and P and in turn how it influences the numerical values of the limits on k_{ij}. The simulation values of k_{ij}, k_{Q1}, k_{Q2}, S_1, S_2, and P (eq 4) are given in Table 1.2. The theoretical limits on the rate constants k_{ij} are also compiled in Table 1.2. For this system, the range of decay time values extends from $\tau_1 = 2.89$ ns and $\tau_2 = 6.09$ ns at [Q] = 0 M to $\tau_1 = 2.14$ ns and $\tau_2 = 3.29$ ns at [Q] = 20 mM and $k_{Q2} = 6$ M^{-1} ns^{-1}. Preexponential factors are positive at low $\tilde{c}_1$ values, but at higher values of $\tilde{c}_1$, the preexponential factors corresponding to the short decay time are negative. The value of k_{01} was kept fixed at different preset values from 0.001 to 0.30 ns^{-1} during the analyses.

4.2.a. $k_{Q1} = 7\ M^{-1}\ ns^{-1}$ *and* $k_{Q2} = 1\ M^{-1}\ ns^{-1}$. Plateaus are found for S_1, S_2, P, k_{Q1}, and k_{Q2} *vs* k_{01} extending up to $k_{01} = 0.16$ ns^{-1} (figure not shown). These visual upper limits are in good agreement with the upper limit on k_{01} calculated according to eq 20a. All the limits on k_{ij} calculated according to eq 20 are compiled in Table 2.2. Also shown are the average k_{Q1} and k_{Q2} values. All those values are in acceptable agreement with the simulation values. For the k_{01} region where plateaus are found, the fits as judged by $Z_{\chi^2_R}$ are acceptable.

4.2.b. $k_{Q1} = 7\ M^{-1}\ ns^{-1}$ *and* $k_{Q2} = 6\ M^{-1}\ ns^{-1}$. Again plateaus are observed for S_1, S_2, P, k_{Q1}, and k_{Q2} up to $k_{01} = 0.16$ ns^{-1} (figure not shown) in good agreement with the upper limit on k_{01} (0.17 ns^{-1}) calculated according to eq 20a using

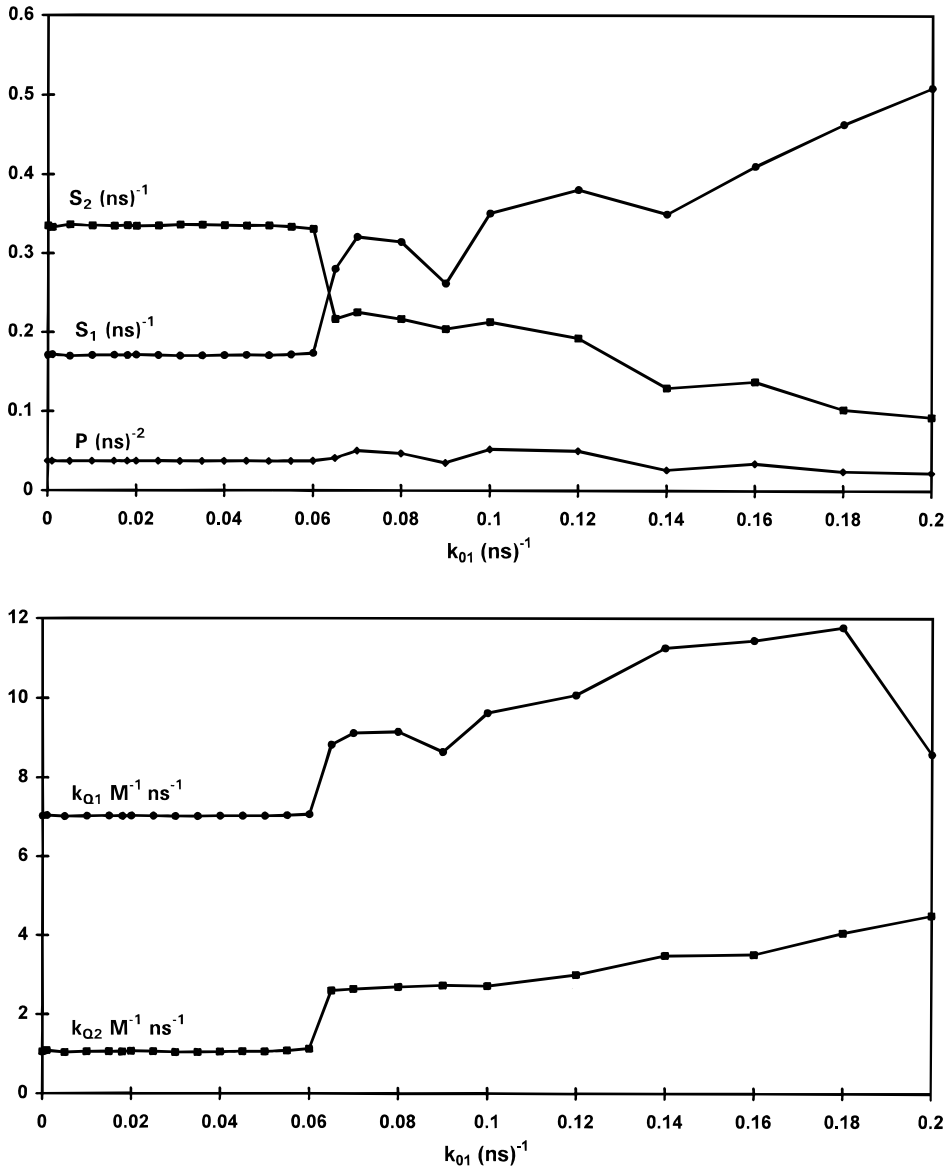

Figure 2. (a) Values of S_1, S_2, and P obtained as a function of the scanned rate constant k_{01} corresponding to case 4.1.a ($S_1 = 0.17$ ns^{-1}, $S_2 = 0.34$ ns^{-1}, $P = 0.0375$ ns^{-2}, $k_{Q1} = 7$ M^{-1} ns^{-1}, and $k_{Q2} = 1$ M^{-1} ns^{-1}). (b) Values of k_{Q1} (●) and k_{Q2} (■) as a function of k_{01} corresponding to the analyses of Figure 2a. The symbols represent actual recovered values, whereas the lines merely serve as a visual aid.

the S_1, S_2, and P values of the plateau. The average values of S_1, S_2, P, k_{Q1}, and k_{Q2} calculated over the plateau and the bounds on k_{ij} are given in Table 3, and they are in acceptable agreement with the respective simulation values (Table 1.2). For the k_{01} range where plateaus are found, the fits are acceptable.

4.3. Systems with $S_1 = 0.17$ ns^{-1}, $S_2 = 0.16$ ns^{-1}, and $P = 0.001$ ns^{-2}. In the present case, S_1 and P are the same as in the previous one but S_1 and S_2 are very similar. The aim is to investigate how the closeness of S_1 and S_2 in combination with a small value of P ($P/S_1S_2 = 0.037$) affects the recovery of S_1, S_2, P, k_{Q1}, and k_{Q2}. The simulation values of k_{ij}, k_{Q1}, k_{Q2}, S_1, S_2, and P are given in Table 1.3. The theoretical limits on the rate constants k_{ij} are also compiled in that table. For this system, the decay time values range from $\tau_1 = 5.08$ ns and $\tau_2 = 7.52$ ns at [Q] = 0 M to $\tau_1 = 3.03$ ns and $\tau_2 = 3.85$ ns at [Q] = 20 mM and $k_{Q2} = 6$ M^{-1} ns^{-1}. At low $\tilde{c}_1$ values, the preexponential factors corresponding to the short decay times are negative, whereas at higher $\tilde{c}_1$ values, all preexponential factors are positive. Rate constant k_{01} was scanned from 0.001 to 0.30 ns^{-1} during the analyses.

4.3.a. $k_{Q1} = 7$ M^{-1} ns^{-1} and $k_{Q2} = 1$ M^{-1} ns^{-1}. The plots of S_1, S_2, P, k_{Q1}, and k_{Q2} as a function of k_{01} (figure not shown) show plateau values up to $k_{01} = 0.14$ ns^{-1}. There is an excellent agreement between the average values of S_1, S_2, P, k_{Q1}, and k_{Q2} and the true values (compare Tables I.3 and II.3). The limits on k_{ij} calculated according to eq 20 are shown in Table 2.3. The limits on k_{ij} are also in very good agreement with the simulation values. There is a small discrepancy between the upper limit on k_{01} calculated by eq 20a (0.162 ns^{-1}) and the visually determined one (0.14 ns^{-1}). The fits are acceptable for the k_{01} range where plateaus are found.

4.3.b. $k_{Q1} = 7$ M^{-1} ns^{-1} and $k_{Q2} = 6$ M^{-1} ns^{-1}. Although plateaus were found for S_1, S_2, P, k_{Q1}, and k_{Q2} as a function of k_{01}, the k_{01} region for constant S_1 and S_2 does not match the k_{01} region where constant k_{Q1} and k_{Q2} values are observed. Furthermore, there is no consistency between the visually determined upper limits on k_{01} and that calculated according to eq 20a. An illustrative example is shown in Figure 5. The visual upper limit on k_{01} determined from the plots of S_1 and S_2 is 0.04 ns^{-1}, while the slightly sloping plots of k_{Q1} and k_{Q2} *vs* k_{01} exhibit a clear break at $k_{01} = 0.14$ ns^{-1}, in good agreement with the upper limit calculated from eq 20a (0.138 ns^{-1}). Because of the inconsistency between the visual and calculated upper limits on the scanned rate constant k_{01}, the results of such

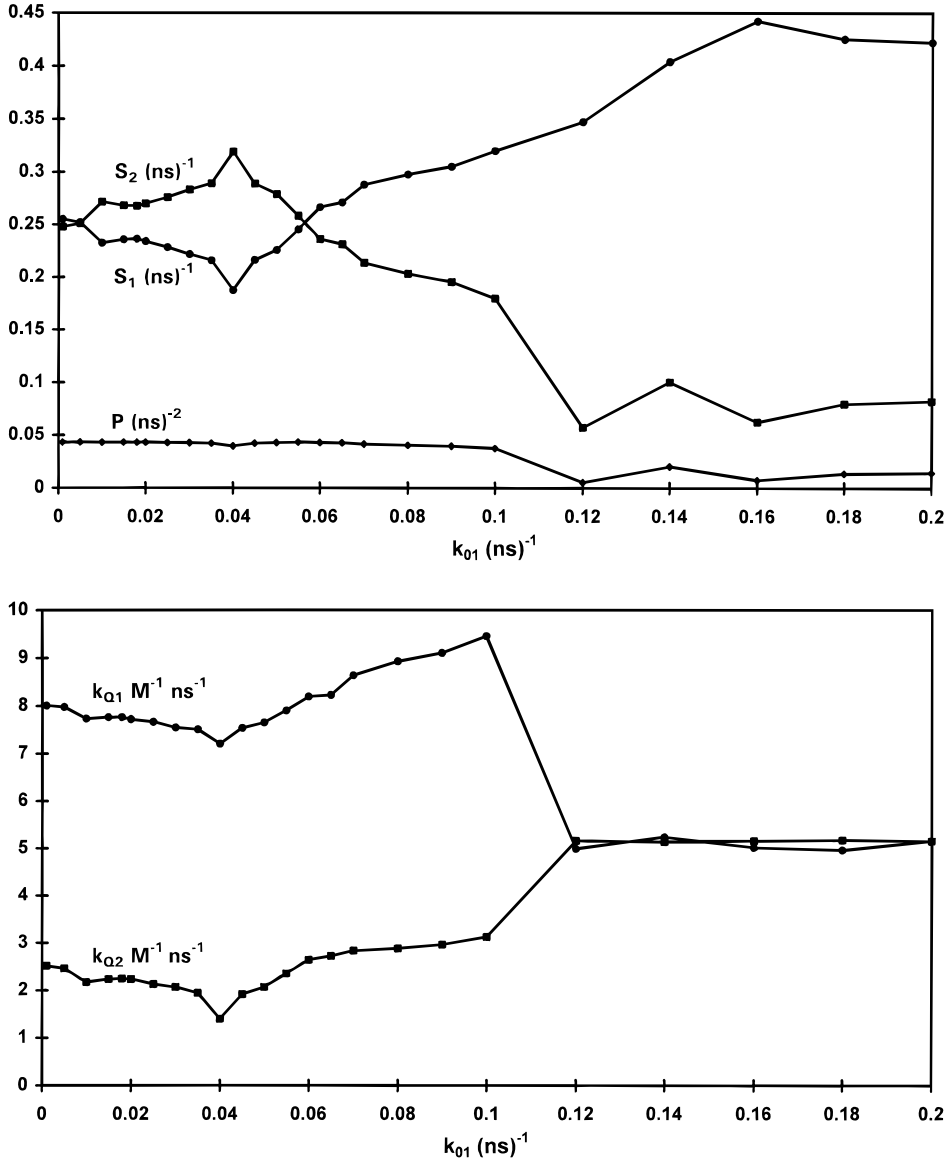

Figure 3. (a) Values of S_1, S_2, and P obtained as a function of the scanned rate constant k_{01} corresponding to case 4.1.a ($S_1 = 0.17$ ns^{-1}, $S_2 = 0.34$ ns^{-1}, $P = 0.0375$ ns^{-2}, $k_{Q1} = 7$ M^{-1} ns^{-1}, and $k_{Q2} = 1$ M^{-1} ns^{-1}), but the [Q] range is limited between 0 and 4 mM. (b) Values of k_{Q1} (●) and k_{Q2} (■) as a function of k_{01} corresponding to the analyses of Figure 3a. The symbols represent actual recovered values, whereas the lines merely serve as a visual aid.

an analysis are not trustworthy. Moreover, the average values of S_1 (0.139 ± 0.003), S_2 (0.189 ± 0.005), and P (0.0003 ± 0.0002) calculated over the plateau ($0.001 \leq k_{01} \leq 0.04$) do not agree with the respective simulation values (Table 1.3). All limits on k_{ij} calculated according to eq 20 are in disagreement with the simulation values (Table 1.3). The analysis of another fluorescence decay surface generated with the same parameters but with different noise yielded extended plateaus of S_1 and S_2 up to $k_{01} = 0.12$ ns^{-1}, whereas the plots of k_{Q1} and k_{Q2} gave a visual upper limit of 0.14 ns^{-1} for k_{01}, different from the upper limit on k_{01} (0.163 ns^{-1}) calculated according to eq 20a. The average values of S_1 (0.169 ± 0.002), S_2 (0.160 ± 0.002), and P (0.0009 ± 0.0001) calculated over the plateau ($0.001 \leq k_{01} \leq 0.12$) and the limits on k_{ij} are in agreement with the respective simulation values (Table 1.3). The average values of k_{Q1} (7.02 ± 0.02) and k_{Q1} (6.01 ± 0.01) agree well with the simulation values.

4.4. Systems with $S_1 = 0.17$ ns^{-1}, $S_2 = 0.80$ ns^{-1}, and $P = 0.0001$ ns^{-2}. The values of S_1 and S_2 are further apart, and P is smaller ($P/S_1S_2 = 0.0007$) than in the previous case. The range of decay time values extends from $\tau_1 = 1.25$ ns, and $\tau_2 = 5.89$ ns at [Q] = 0 M to $\tau_1 = 1.09$ ns and $\tau_2 = 3.23$ ns at [Q] = 20 mM and $k_{Q2} = 6$ M^{-1} ns^{-1}. All preexponential factors are positive, but when the value of $\tilde{c}_1$ is 1.0, the preexponential factors corresponding to the short decay time are negative. The value of k_{01} was kept constant at different preset values from 0.001 to 0.30 ns^{-1} during the scanning procedure.

4.4.a. $k_{Q1} = 7$ M^{-1} ns^{-1} and $k_{Q2} = 1$ M^{-1} ns^{-1}. Well-defined plateaus are found for S_1, S_2, P, k_{Q1}, and k_{Q2} *vs* k_{01} extending up to $k_{01} = 0.17$ ns^{-1}, corresponding to the upper limit on k_{01} calculated according to eq 20a. All of the limits on k_{ij} calculated according to eq 20 are shown in Table 2.4, together with the average k_{Q1} and k_{Q2} values. All those values are in excellent agreement with the simulation values. Acceptable fits are obtained for the k_{01} range where plateaus are found.

4.4.b. $k_{Q1} = 7$ M^{-1} ns^{-1} and $k_{Q2} = 6$ M^{-1} ns^{-1}. Although plateaus are observed for S_1, S_2, P, k_{Q1} and k_{Q2}, the visual upper limits on k_{01} are different when they are derived from the (S_1, S_2, P) plot *vs* k_{01} (namely 0.12 ns^{-1}) than from k_{Q1} *vs* k_{01} (namely 0.18 ns^{-1}) or from k_{Q2} *vs* k_{01} (namely 0.04 ns^{-1}). All visually obtained limits are in disagreement with the upper limit on k_{01} (0.17 ns^{-1}) calculated according to eq 20a. The average values

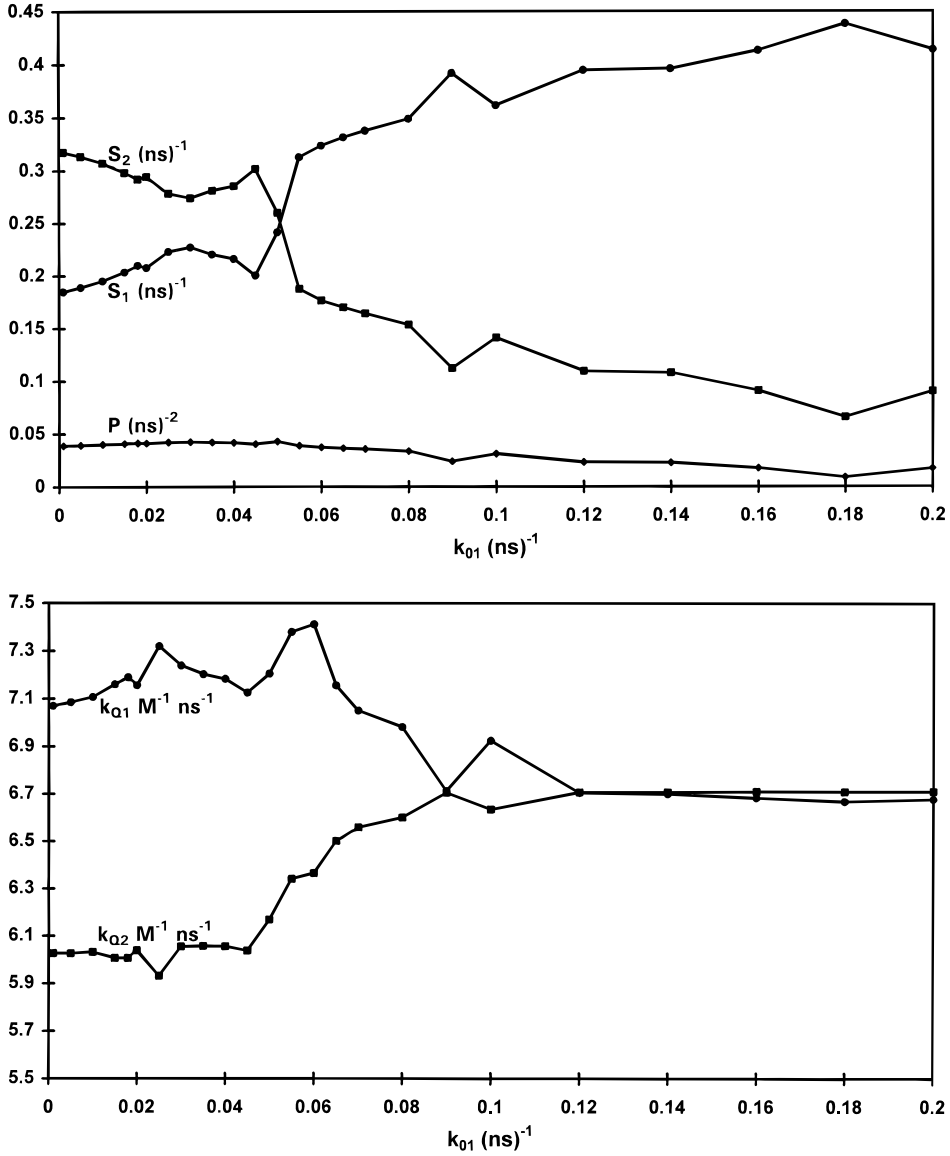

Figure 4. (a) Values of S_1, S_2, and P obtained as a function of the scanned rate constant k_{01} corresponding to case 4.1.b ($S_1 = 0.17$ ns^{-1}, $S_2 = 0.34$ ns^{-1}, $P = 0.0375$ ns^{-2}, $k_{Q1} = 7$ M^{-1} ns^{-1}, and $k_{Q2} = 6$ M^{-1} ns^{-1}). (b) Values of k_{Q1} (●) and k_{Q2} (■) as a function of k_{01} corresponding to the analyses of Figure 4a. The symbols represent actual recovered values, whereas the lines merely serve as a visual aid.

of S_1 (0.17 ± 0.01), S_2 (0.80 ± 0.03), and P (0.0007 ± 0.0004) and the limits on k_{ij} are in agreement with the respective simulation values (Table 1.4). The values of k_{Q1} and k_{Q2} are 7.02 ± 0.01 and 6.7 ± 0.3 M^{-1} ns^{-1}, respectively.

4.5. Systems with $S_1 = 0.17$ ns^{-1}, $S_2 = 0.80$ ns^{-1}, and $P = 0.1008$ ns^{-2}. Compared to the previous case, the value of P is much larger ($P/S_1S_2 = 0.74$). For this system, the decay time values extend from $\tau_1 = 1.07$ ns and $\tau_2 = 26.48$ ns at [Q] = 0 M to $\tau_1 = 0.95$ ns and $\tau_2 = 5.72$ ns at [Q] = 20 mM and $k_{Q2} = 6$ M^{-1} ns^{-1}. At low $\tilde{c}_1$ values, all preexponential factors are positive, whereas at higher $\tilde{c}_1$ values, the preexponential factors corresponding to the short decay time are negative. The value of k_{01} was kept constant at different preset values from 0.001 to 0.20 ns^{-1} during the analyses.

4.5.a. $k_{Q1} = 7\ M^{-1}\ ns^{-1}$ and $k_{Q2} = 1\ M^{-1}\ ns^{-1}$. Plots of S_1, S_2, P, k_{Q1}, and k_{Q2} *vs* the scanned rate constant k_{01} exhibit plateaus up to $k_{01} = 0.04$ ns^{-1}. This visual upper limit on k_{01} agrees well with that obtained by eq 20a (0.044 ns^{-1}). Table 2.5 compiles the values of S_1, S_2, P, k_{Q1}, and k_{Q2} averaged over the plateau region. The limits on k_{ij} calculated according to eq 20 are also compiled in this table. All those values are in good agreement with the simulation values.

4.5.b. $k_{Q1} = 7\ M^{-1}\ ns^{-1}$ and $k_{Q2} = 6\ M^{-1}\ ns^{-1}$. In contrast to case 4.5.a., no plateaus are obtained for S_1, S_2, P, k_{Q1}, and k_{Q2} as a function of k_{01}.

5. Discussion

From the global compartmental analyses of computer-generated fluorescence decay surfaces of reversible intramolecular two-state excited-state processes with added quencher, it can be concluded that the closeness of the values of the two quenching rate constants influences the reliability of the recovered values of S_1, S_2, P, k_{Q1}, and k_{Q2} and the limits on k_{ij}.

(i) If the values of the rate constants of quenching k_{Q1} and k_{Q2} are substantially different, plateaus are observed for S_1, S_2, P, k_{Q1}, and k_{Q2} as a function of the scanned rate constant, provided a wide enough [Q] range is selected. The values of those parameters averaged over the plateaus are in good agreement with the respective simulation values. Furthermore, the upper limits on the scanned rate constant obtained by visual inspection of the individual plateaus agree with each other and with that calculated according to eq 20 and with the simulated one (according to eq 10). Moreover, the bounds on all k_{ij} calculated according to eq 20 using the plateau values of S_1,

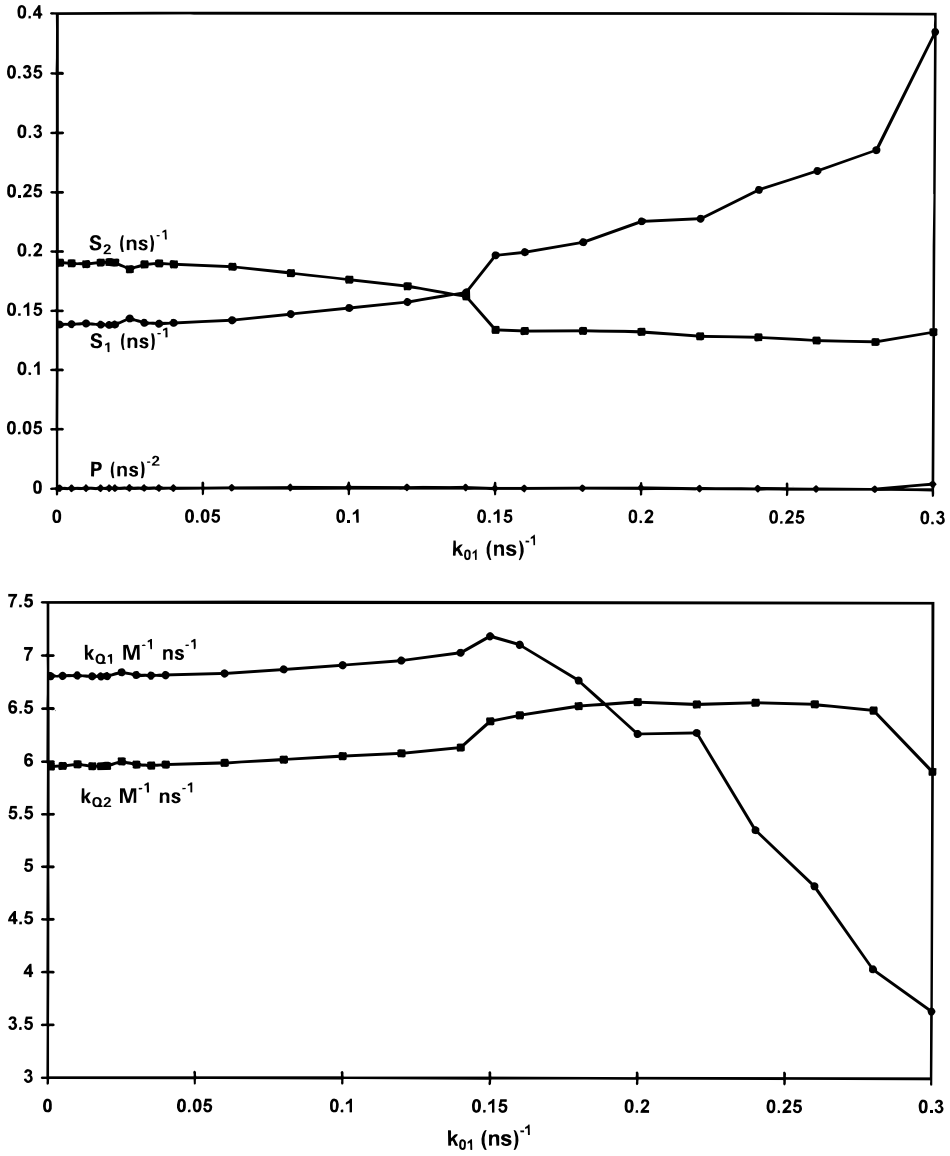

Figure 5. (a) Values of S_1, S_2, and P obtained as a function of the scanned rate constant k_{01} corresponding to case 4.3.b ($S_1 = 0.17$ ns^{-1}, $S_2 = 0.16$ ns^{-1}, $P = 0.001$ ns^{-2}, $k_{Q1} = 7$ M^{-1} ns^{-1}, and $k_{Q2} = 6$ M^{-1} ns^{-1}). (b) The values of k_{Q1} (●) and k_{Q2} (■) as a function of k_{01} corresponding to the analyses of Figure 5a. The symbols represent actual recovered values, whereas the lines merely serve as a visual aid.

S_2, and P agree well with the simulation values calculated according to eq 10. Hence, the scanning procedure can be used to recover reliable estimates of the limits on all rate constants.

(ii) If the values of k_{Q1} and k_{Q2} are very similar, the quality of recovery of S_1, S_2, P, k_{Q1}, and k_{Q2} depends on several factors. It is possible that no plateaus are found for S_1, S_2, P, k_{Q1}, and k_{Q2} as a function of the scanned rate constant. This situation occurs when P is nonnegligible in comparison with the product S_1S_2 (see eq 17), as was found in sections 4.1b and 4.5 b. This is a clear-cut case because no information can be extracted from the scanning procedure. The only remedy is to select another quencher with widely differing quenching rates. If plateaus are found for the parameters S_1, S_2, P, k_{Q1}, and k_{Q2}, two cases can be distinguished. First, when all the plateaus yield the same visual upper bound on the scanned rate constant (which corresponds to that calculated according to eq 20 using the plateau values of S_1, S_2, and P), then the limits on all rate constants k_{ij} are recovered correctly. This was found for case 4.2b. Second, when different visual upper limits for the scanned rate constant are obtained from the plateaus of S_1, S_2, P, k_{Q1}, and k_{Q2} (and at least one of them is different from that calculated from eq 20, the obtained results of the analysis are not reliable. That was found in cases 4.3b and 4.4b. The choice of another quencher with widely spaced k_{Q1} and k_{Q2} is required. It should be emphasized that the analyses giving unreliable limits never passes our consistency test. It may happen, however, that some analyses yielding reliable estimates of S_1, S_2, P, k_{Q1}, and k_{Q2} will be rejected.

On the basis of the results of this investigation, the following strategy for experimental design can be suggested. When studying intramolecular two-state excited-state processes with added quencher, one should determine in a trial experiment how closely spaced the rate constants of quenching are. For this purpose one can collect a minimum of three decay traces at three different quencher concentrations at the same excitation/emission wavelength. Inclusion of a decay trace in the absence of added quencher ensures the largest possible range of decay times. From the structural identifiability study, it follows that a straightforward global compartmental analysis with k_{01} fixed at zero guarantees that the rate constants k_{ij}, k_{Q1} and k_{Q2} are uniquely determined.[20] Moreover, this analysis gives an indication of the closeness of the values of the two quenching rate constants and yields the dependence of the decay times on [Q], allowing one to select the appropriate quencher concentration range. Note that it is not always beneficial to use the widest possible [Q] range. Indeed, as can be seen from Figure 1, using

[Q] higher than 0.05 M will not cause a large change in $\tau_{1,2}$. As shown in case 4.1.b., extension of the [Q] range up to 0.1 M was not helpful in obtaining reliable values of S_1, S_2, and P.

For the the proximity of the quenching rate constants two cases can be considered: (i) If the values of the quenching rate constants are well separated, one can collect the fluorescence decay curves under the right experimental conditions using a suitable quencher concentration range. Based on the simulations, one can predict that global compartmental analysis with k_{01} scanned will yield plateaus for S_1, S_2, P, k_{Q1}, and k_{Q2} as a function of k_{01}. If no plateaus are found, one should expand the [Q] range to increase the spread of $\tau_{1,2}$ values. Eventually, correct values of k_{Q1} and k_{Q2} and limits on k_{ij} will be obtained.

(ii) If the quenching rate constants are closely spaced in value, one should compare the P value with the product S_1S_2. If P is nonnegligible, one should search for another quencher which quenches the two excited states with very differing efficiencies. If P is small, one can try performing the scanning procedure to determine S_1, S_2, P, k_{Q1}, and k_{Q2} as a function of k_{01}. If the visual upper limits are not internally consistent and/or different from that calculated according to eq 20, the results are not reliable and one should start anew with a different quencher.

References and Notes

(1) Beechem, J. M.; Ameloot, M.; Brand, L. *Chem. Phys. Lett.* **1985**, *120*, 466−472.

(2) Ameloot, M.; Beechem, J. M.; Brand, L. *Chem. Phys. Lett.* **1986**, *129*, 211−219.

(3) Ameloot, M.; Boens, N.; Andriessen, R.; Van den Bergh, V.; De Schryver, F. C. *J. Phys. Chem.* **1991**, *95*, 2041−2047.

(4) Andriessen, R.; Boens, N.; Ameloot, M.; De Schryver, F. C. *J. Phys. Chem.* **1991**, *95*, 2047−2058.

(5) Khalil, M. M. H.; Boens, N.; Van der Auweraer, M.; Ameloot, M.; Andriessen, R.; Hofkens, J.; De Schryver, F. C. *J. Phys. Chem*. **1991**, *95*, 9375−9381.

(6) Andriessen, R.; Ameloot, M.; Boens, N.; De Schryver, F. C. *J. Phys. Chem.* **1992**, *96*, 314−326.

(7) Ameloot, M.; Boens, N.; Andriessen, R.; Van den Bergh, V.; De Schryver, F. C. *Methods Enzymol.* **1992**, *210*, 314−340.

(8) Van den Bergh, V.; Boens, N.; De Schryver, F. C.; Ameloot, M.; Gallay, J.; Kowalczyk, A. *Chem. Phys.* **1992**, *166*, 249−258.

(9) Khalil, M. M. H.; Boens, N.; De Schryver, F. C. *J. Phys. Chem*. **1993**, *97*, 3111−3122.

(10) Van den Bergh, V.; Kowalczyk, A.; Boens, N.; De Schryver, F. C. *J. Phys. Chem.* **1994**, *98*, 9503−9508.

(11) Hermans, B.; De Schryver, F. C.; Boens, N.; Ameloot, M.; Jérôme, R.; Teyssié, P.; Goethals, E.; Schacht, E. *J. Phys. Chem.* **1994**, *98*, 13583−13593.

(12) Van den Bergh, V.; Boens, N.; De Schryver, F. C.; Ameloot, M.; Steels, P.; Gallay, J.; Vincent, M.; Kowalczyk, A. *Biophys. J*. **1995**, *68*, 1110−1119.

(13) Hermans, B.; De Schryver, F. C.; van Stam, J.; Boens, N.; Jérôme, R.; Teyssié, P.; Trossaert, G.; Goethals, E.; Schacht, E. *Macromolecules* **1995**, *28*, 3380−3386.

(14) Van den Bergh, V.; Boens, N.; De Schryver, F. C.; Gallay, J.; Vincent, M. *Photochem. Photobiol.* **1995**, *61*, 442−447.

(15) Meuwis, K.; Boens, N.; De Schryver, F. C.; Gallay, J.; Vincent, M. *Biophys. J.* **1995**, *68*, 2469−2473.

(16) Kowalczyk, A.; Meuwis, K.; Boens, N.; De Schryver, F. C. *J. Phys. Chem*. **1995**, *99*, 17349−17353.

(17) Meuwis, K.; Depuydt, G.; Boens, N.; De Schryver, F. C. *Chem. Phys. Lett.* **1995**, *246*, 641−648.

(18) Boens, N.; Kowalczyk, A.; Cielen, E. *J. Phys. Chem*. **1996**, *100*, 4879−4887.

(19) Boens, N.; Andriessen, R.; Ameloot, M.; Van Dommelen, L.; De Schryver, F. C. *J. Phys. Chem.* **1992**, *96*, 6331−6342.

(20) Boens, N.; Ameloot, M.; Hermans, B.; De Schryver, F. C.; Andriessen, R. *J. Phys. Chem.* **1993**, *97*, 799−808.

(21) Boens, N.; Van Dommelen, L.; Ameloot, M. *Biophys. Chem.* **1993**, *48*, 301−313.

(22) Van Dommelen, L.; Boens, N.; Ameloot, M.; De Schryver, F. C.; Kowalczyk, A. *J. Phys. Chem.* **1993**, *97*, 11738−11753.

(23) Van Dommelen, L.; Boens, N.; Ameloot, M.; De Schryver, F. C. *J. Phys. Chem.* **1995**, *99*, 8959−8971.

(24) van Stam, J.; Van Dommelen, L.; Boens, N.; Zachariasse, K.; De Schryver, F. C. *J. Phys. Chem.* **1995**, *99*, 9386−9396.

(25) Knutson, J. R.; Beechem, J. M.; Brand, L. *Chem. Phys. Lett.* **1983**, *102*, 501−507.

(26) Beechem, J. M.; Ameloot, M.; Brand, L. *Anal. Instrum. (NY)* **1985**, *14*, 379−402.

(27) Löfroth, J. -E. *Eur. Biophys. J.* **1985**, *13*, 45−58.

(28) Ameloot, M.; Beechem, J. M.; Brand, L. *Biophys. Chem.* **1986**, *23*, 155−171.

(29) Janssens, L. D.; Boens, N.; Ameloot, M.; De Schryver, F. C. *J. Phys. Chem.* **1990**, *94*, 3564−3576.

(30) Boens, N.; Janssens, L. D.; De Schryver, F. C. *Biophys. Chem.* **1989**, *33*, 77−90.

(31) Marquardt, D. W. *J. Soc. Ind. Appl. Math.* **1963**, *11*, 431−441.

(32) Boens, N. In *Luminescence Techniques in Chemical and Biochemical Analysis*; Baeyens, W. R. G., De Keukeleire, D., Korkidis, K., Eds.; Marcel Dekker: New York, 1991; pp 21−45.

(33) Van den Zegel, M.; Boens, N.; Daems, D.; De Schryver, F. C. *Chem. Phys.* **1986**, *101*, 311−335.